Chapter 15

Building of Open-Structure Wheel-Based Mobile Robotic Platform

The chapter describes the development of an open-structure wheel-based mobile robotic platform and a complementary software simulator aimed at research, development and education, as well as the objective benchmarking of this kind of advanced mechatronic system. The main objectives of the work are concerned with solving the problems of development of an autonomous navigation system, motion planning and control of mobile robots in unstructured environments in the presence of mobile and immobile obstacles and system uncertainties such as a variation in tire–ground interaction.

15.1. Introduction

Mobile robots are subjected to many recent research studies [MOR 08, MIN 08] with aim to provide reliable and robust robotic platforms for broad service applications at home, in the office, in public institutions, etc. Mobile robotic platforms make the basis for the building of advanced mechatronic devices such as ambiently intelligent service robots. These systems are expected to be widely utilized in the future in everyday human life, but still many challenges remain to be overcome [HAB 06]. The problems in building such advanced intelligent systems are predominantly related to the success

---

Chapter written by Aleksandar RODIĆ and Ivan STOJKOVIĆ.

of solving complex perceptive, cognitive and control tasks related to advance sensing, wireless communication, environmental understanding, trajectory planning as well as adaptation to variable environmental conditions. In that sense, the main tasks to be solved with mobile robots are the development of algorithms for spatial reasoning, autonomous navigation, motion planning and reliable control of system dynamics in conditions of unknown, unpredicted and evolving environments. Therefore, an open-structure mobile robotic platform (a small experimental model, i.e. test-bed station) and corresponding software simulator are needed to support research and education in this field of mechatronics. Accordingly, this chapter deals with the building of such an open-structure test-bed system. Complementary to system development, a hybrid knowledge-based and model-based controller of the robotic system is also designed. The controller developed and integrates navigation and a control module into the unique control architecture designed to enable intelligent system navigation and dynamic control of a wheeled robot in the presence of system uncertainties.

This chapter is organized in the following way. Section 15.2 gives a brief state of the art regarding methods and techniques of advanced navigation and control of autonomous mobile robots. The architecture of the experimental, open-structure wheel-based mobile robotic platform is described in section 15.3. Kinematical and dynamic modeling of the robot system and building of the complementary user-oriented, open-source software simulator dedicated to research and system analysis are presented in section 15.4. Section 15.5 is dedicated to synthesis of advance motion planning and control algorithms. In section 15.6, the simulation and experimental tests are described and the results are analyzed with an aim to validate the proposed algorithms. Section 15.7 gives concluding remarks and some remarks concerning implementation aspects of the open-structure robotic platform. The chapter is finalized by expressing acknowledgments and providing a list of references.

15.2. State of the art

Numerous research studies concerning control of wheeled mobile robots were reported in [MOR 08, MIN 08]. In particular, non-holonomy constraints associated with these systems have motivated the development of highly nonlinear control techniques. For the sake of simplicity, the control methods are developed mainly for unicycle-type and car-like mobile robots. Most of the results can, in fact, be extended to other types of mobile robots (e.g. holonomic), in particular to the systems with trailers. A complementary problem to control the motion of mobile robots is also concerned with global

motion planning and obstacle (mobile and immobile) avoidance in a variety of different static as well as dynamic scenarios (e.g. interaction of several robots). The problem considers sensor-based motion to face the physical issues of real system navigation in a real world. The problem relates to searching for the techniques, how to navigate toward a goal in a confined, troublesome or cluttered environment when the obstacles to avoid are discovered in real time? This is the question that addresses simultaneous motion planning and control as well as obstacle avoidance.

The methods that combine both the global point of view of motion planning and the local point of view of obstacle avoidance have already been developed. How can we consider robot perception at the planning level? This is the so-called sensor-based motion planning. Several variants exist, such as the "bug algorithms" initially introduced in [LUM 87]. However, none of them consider the practical context of non-holonomic mobile robots.

Obstacle avoidance techniques and methods can be categorized in two groups according to [MOR 08]: methods that compute the motion in one step and that do it in more than one step. One-step methods directly reduce the sensor information to a motion control. There are two types of methods:

– The heuristic methods were the first techniques used to generate motion based on sensors. The majority of these works are derived from classic planning methods [LUM 87, CHA 82, STR 84, CHA 85].

– The methods of physical analogies assimilate the obstacle avoidance to a known physical problem. The representatives of these are the potential field methods [KHA 86, KRO 86]. Other works are variants adapted to uncertain models [BOR 89] or that use other analogies [AZA 94, MAS 94, SIN 96].

Methods with more than one step compute some intermediate information, which is processed next to obtain the motion.

– The methods of a subset of controls compute an intermediate set of motion controls, and next choose one of them as a solution. There are two types: (1) methods that compute a subset of motion directions. The vector field histogram [BOR 91] and the obstacle restriction method [MIN 05] can be mentioned as the examples. Another method is presented in [FEI 94]. (2) Methods that compute a subset of velocity controls. The dynamic window approach [FOX 97] and the velocity obstacles [FIO 98] can be taken as examples. Another method based on similar principles but developed independently is the curvature velocity method [SIM 96].

– Finally, there are methods that compute some high-level information as intermediate information, which is translated next in motion. The nearness navigation diagram [MIN 00, MIN 04] is the representative of this method.

Regarding the control techniques applied with mobile robots, there are also several ways applied in engineering practice. Besides Ackermann [WIK], and differential steering, skid steering is the most popular and widely used steering method for wheeled and tracked vehicles. The skid steering mechanism provides high mobility and maneuverability due to strong traction, which makes it suitable for all-terrain traversal. While in differentially steering robots, assumption of no slip can be used to derive adequate models and control laws, this is not the case with skid steering robots, because of higher influence of slip on robot motion. This makes modeling of dynamics and kinematics more difficult, since complex wheels and terrain interaction needs to be accounted in the model, in order to accurately describe the motion of a skid steering robot.

In [CAR 99], a dynamic model for planar motion was developed and it was used to design a feedback linearization based controller for trajectory tracking. A similar dynamic model with the addition of actuator dynamics was introduced in [KOZ 04] and a controller was devised using the back-stepping technique. The property of differential flatness was utilized in [RYU 11] to derive a robust trajectory tracking controller for wheeled mobile robots based on a dynamic and kinematic model with slip. In [YI 07], a pseudo-static friction model is used to capture the interaction between the wheels and ground, and to further develop a dynamic model of a skid-steered wheeled vehicle. Also, an adaptive controller is designed to enable the robot to follow a desired trajectory. The inputs of the dynamic model are the longitudinal slip ratios of the four wheels. Since longitudinal slip ratios are difficult to measure in practice, there is a need for their estimation. A model-based approach for longitudinal slip estimation was introduced in [WAR 08], where a novel tire traction/braking model is presented and used to calculate vehicle dynamic forces in an extended Kalman filter framework.

To summarize the previous consideration, the use of an obstacle avoidance technique with mobile robots in a given scenario is highly dependent on the scenario's nature (static or dynamic, unknown or known, structured or not or its size, for example). Usually, this problem is associated with the integration of motion planning and obstacle avoidance. All the methods outlined in this section have certain advantages as well as disadvantages depending on the navigation context, like uncertain

environments, motion at high speeds and motion in confined or troublesome spaces. Unfortunately, there is no objective metrics available to benchmark the performance of the variety of navigation and control methods in a quantitative way. In that sense, the considerations performed in this chapter represent a contribution to the development of one such mini-benchmarking system, which is open structured, user-oriented and scalable.

15.3. Configuring of the experimental system

The experimental open-structure wheel-based mobile robotic platform is shown in Figure 15.1. It has a modular structure that consists of the following subsystems (modules): (1) four-wheel drive rover, (2) five degrees of freedom (DoF) robot arm for small objects manipulation, (3) IP stereo-vision camera, (4) advanced sensorial system including different localization and navigation sensors (visual and non-visual), (5) PC-based on-board controller and (6) Wi-Fi communication module. A Hagisonic StarGazer optical sensor unit [STA 11] is used as an additional, external module for global localization of the robotic system in the workspace. The high-level system description is presented in Figure 15.2 and the particular modules are described in more detail in the following sections.

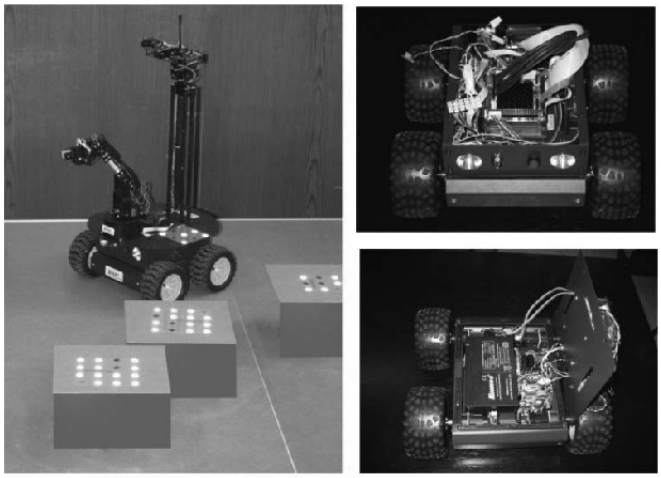

a) b)

Figure 15.1. *a) Assembled 4WD rover; b) Hardware configuration: control and acquisition boards (up) and battery with power-electronics (down). For a color version of this figure please see www.iste.co.uk/mechatroneng.zip*

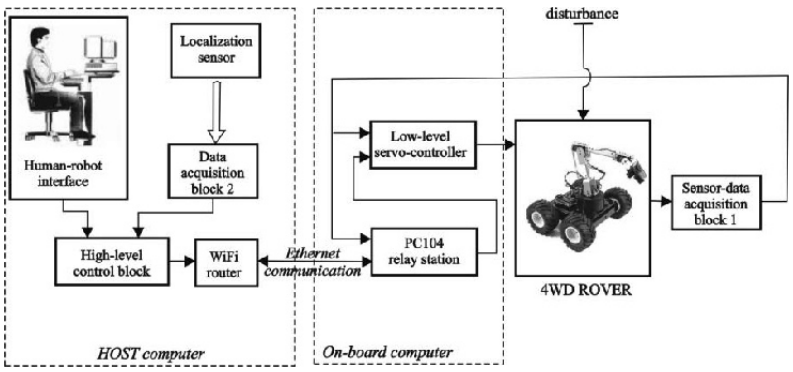

Figure 15.2. *High-level system description*

15.3.1. *Wheel-based mobile robot*

The DFRobot 4WD outdoor mobile platform (Figure 15.1) is a small 4WD rover of 6.8 kg payload designed for the research purposes [DFR 11]. The robot is supported by four wheels that are driven in a differential configuration. The wheels are powered by geared direct current (DC) motors with mounted incremental encoders. The sensory system of the mobile platform consists of infrared (IR) and ultrasound proximity sensors as well as an three-axis gyroscope and an three-axis accelerometer. A five-DoF robot arm AL5A [LYN 11] is mounted on the mobile platform. It is powered by 5 RC servo-motors. The control system of the mobile platform (Figure 15.3) is based on the master PC-104 board [ADL 11] and a slave board for control of the RC servo/motors. A PC-104 board is powered by an Intel® Atom™ processor 512 MB RAM, and 2 GB SSD flash drive master board also contains a bundle of interfaces: USB, RS232 and connectors to various peripheral boards. In addition, a USB-to-Wi-Fi adaptor is used for wireless communication with main computer.

15.3.2. *System for localization and obstacle detection*

StarGazer [STA 11] is chosen as an indoor localization system appropriate for this project. An on-board DSP processes an IR image, which is reflected from passive landmarks on the scene. Each landmark has a unique ID. Outputs from the processing unit are the position and the heading angle of the landmark. The system is rather accurate (error less than 1 cm), reliable and resistant to fluorescent light and sunshine. Stargazer is connected to the PC server via RS232 bus.

The basic tasks of navigation and control of mobile robotic systems are tasks of obstacle and collision avoidance. For that purpose, with the 4WD rover (Figure 15.1), two kinds of sensors are implemented: (1) Mindsensors [MIN 11] – a high-precision medium range (1.5 m) IR distance sensor, and (2) Devantech [DEV 11] – a SRF10 ultrasonic scanning range finder for detection proximity of obstacles and mapping environment. The robot is equipped with a wireless IP stereo-vision system [SUR 11].

15.3.3. *Architecture of the on-board controller*

The control architecture is shown in Figure 15.3. The mobile robot controller consists of the following elements: a ADLS15PC – Intel® Atom™ CPU 1.60 GHz PC104 processor board, a PC104 acquisition board, a ENCDA PC104 analog encoder board, a DIGIO PC104 universal board, a DC–DC converter block that provides power supply for the system, a motor driver, a robotic arm and a stereo camera controller, a network of ultrasonic and IR sensors, integrated three-axis accelerometer and three-axis gyroscope.

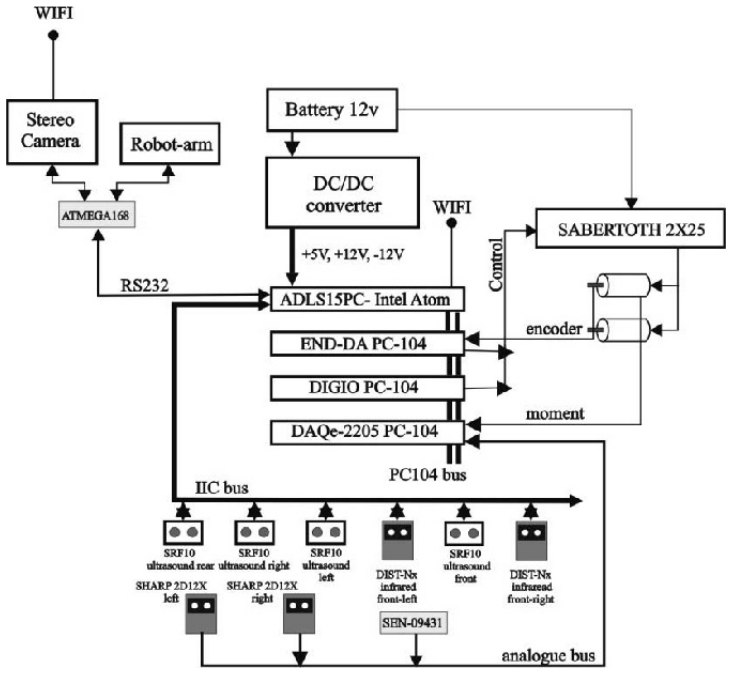

Figure 15.3. *Architecture of the system on-board controller*

The PC104 controller has the following characteristics: Intel® Atom™, dual core processor, 1.60 GHz operating frequency, Intel SCH US15W Chipset, 1 GB DDR2-DRAM, CRT/LVDS Interface Onboard, 10/10/1000 Base-T Ethernet, 8 × USB2.0 orts, PATA Storage Interface, COM1, COM2, LPT1, SM Bus Interface, RTC and Watchdog Timer, High-Definition Audio, 4 GB On-board SSD. A UBUNTU RTC operating system has been installed to perform monitoring and control of the whole system, to receive commands from a base station via Wi-Fi network paths and to execute received commands. An encoder and digital to analog output (ENCDA) universal board has been developed specifically to provide motor control and acceptance of signals from the encoder. A digital input-output (DIGIO) PC104 universal board was designed to allow reading of 16 digital optically isolated general purpose signals and activation of eight digital outputs that might be configured differently (PNP type tranistor, NPN type transistor, NMos and Relay). In the robot controller, the DIGIO board was used for control of the lights on the robot and control of the operating voltage for the motor driver and robotic arm driver. The SABERTOOTH 2 × 25 driver is used as the motor driver since it provides independent control of two motors simultaneously. As a control signal for the driver, voltage signal from −10 to 10 V is used, by which the driver generates the appropriate output (voltage and current) to the motor joint.

A network of embedded IR and ultrasonic obstacle detectors provides simultaneous and independent reading and detection of the obstacles within a 360° circle. Obstacle sensors are implemented in a network through a standard IIC bus implemented on the LPT1 port, as well as through direct reading of the sensor connected to acquisition card. Acquisition card DAQe-2205 features are as follows: Analog 64 single-ended inputs or 32 differential inputs; resolution/sample rate 16-bit at 500 kS/s; input ranges: unipolar 0 to +1.25, +2.5, +5 and +10 V; bipolar ±1.25, ±2.5, ±5 and ±10 V; A/D FIFO size 1,024 samples; trigger modes pre-/post-/middle-/delay-/repeat-trigger; analog outputs: two 12-bit waveform generation channels; 1 MS/s update rate; output ranges: 0 to +10, ±10 V, 0 to AOEXTREF, ±AOEXTREF; D/A FIFA size 1,024 samples; digital I/O 24 lines (82C55) all boards; counter/timer: two 16-bit counter/timers. With a PC104 acquisition card it is possible to measure and monitor the current of the vehicle motors and thus perform more advanced control techniques of the vehicle based on the position as well as on the force in the wheels. This acquisition card is connected to the following sensors: the three-axis accelerometer and the three-axis gyroscope SEN-09431 and two side IR sensors SHARP 2D12X. An inertial sensor has the following characteristics: pitch, yaw and roll gyro outputs, 1 × and 4 × amplified (0.83 and 3.33 mV/°/s sensitivity,

respectively) ±300°/s range, *x*-, *y*- and *z*-axis accelerometer outputs, 300 mV/g sensitivity, ±3 g range; all necessary filtering components, access to gyro's self-test, power down and high-pass filter reset pins. The IR obstacle sensor use the IR signal to measure object distance from 10 to 80 cm with analog output. It has been mounted on the sides of the vehicle to detect obstacles in the space on the left and right. The sensors network on the IIC bus consists of four SRF10 ultrasonic obstacle detectors mounted on all four sides of the vehicle, and two IR obstacle sensors DIST Ns medium-V2.

Maximum range of the SRF10 is set by an internal timer. By default, this is 65 ms or the equivalent of 11 m in range. This is much further than 6 m for which SRF10 is actually capable. It is possible to reduce the time that the SRF10 takes to detect an echo, and hence the range, by writing to the range register at location 2. The range register can be set in steps of about 43 mm (0.043 m or 1.68 in) up to 11 m. The range is ((range register × 43 mm) + 43 mm), so setting the range register to 0 (0 × 00) gives a maximum range of 43 mm. Setting the range register to 1 (0 × 01) gives a maximum range of 86 mm. More usefully, 24 (0 × 18) gives a range of 1 m and 93 (0 × 5D) gives of 4 m. Setting 255 (0 × FF) gives the original 11 m (255 × 43 + 43 is 11,008 mm). An IR obstacle sensor DIST-Nx is an optical distance sensor (various SHARP sensors) with digital (IIC) interface. This can be used to measure precise distances from an obstacle. The distance range of sensor variants is medium range: 10–80 cm (with the highest precision in a zone ranging from 10 to 40 cm). The sensor detects distance based on the angle of arriving reflected IR. The sensor is mounted on the front angles of the vehicle.

A controller using RS232 interface controls the robotic arm that is mounted on the front of the vehicle. The robotic arm has five DoF as well as a service grab. The RC servo motors were used in the arm. The microcontroller, ATMEL ATMEGA168-20PU, directly controls RC servo motors by generating a pulse width modulation (PWM) signal with a period of 20 ms for each DoF. This microcontroller controls a pan-tilt stereo camera module Surveyor Stereo Vision System (SVS) SRV-1 Blackfin [SUR 11], as well. This is achieved through a serial RS232 link, with the band rate of 19,200. The schematic representation of the controller is given in Figure 15.2.

The complete system consists of two mutually connected modules communicated by Wi-Fi interface. A 4WD rover with on-board control is subordinated to the high-level control module installed at the host computer (basis station) as shown in Figure 15.3. A corresponding graphical user interface (GUI) ensures remote monitoring, that is supervisory control and data acquisition.

15.4. Modeling and simulation of the system

For designing of control algorithms and their validation, prior to an experimental testing, appropriate modeling of the wheeled robot (Figure 15.1) with differential (skid) steering capabilities is done. A corresponding software simulator is built based on the model developed. A nonlinear model of the 4WD rover is assumed as an appropriate representative that takes into account the robot capability to move on a sloped surface, too. The appropriate model that fits the system's physical capabilities in a satisfactory accurate way is presented in Figures 15.4 and 15.5. In a general case, it is assumed that the surface slope appears in both longitudinal γ_x as well as lateral γ_y direction of motion as shown in Figure 15.5. A complementary kinematical model of rover tires is presented in Figure 15.4, too. Special attention in this chapter is dedicated to modeling of nonlinear tire dynamics. The importance of parameter estimation of tire–ground adhesion will be emphasized, too. Both the extremely nonlinear nature of rubber tires and the corresponding parametric uncertainties regarding tire rolling and slipping during skid steering maneuvers are considered in this chapter. In the following sections, appropriate modeling of 4WD robot kinematics and dynamics is presented.

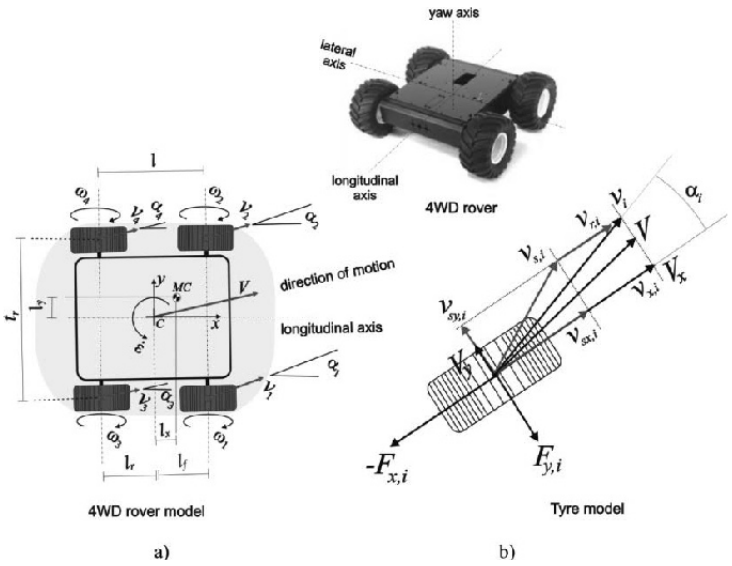

Figure 15.4. *a) Kinematical model of 4WD rover considered in this chapter and b) corresponding tire kinematical model*

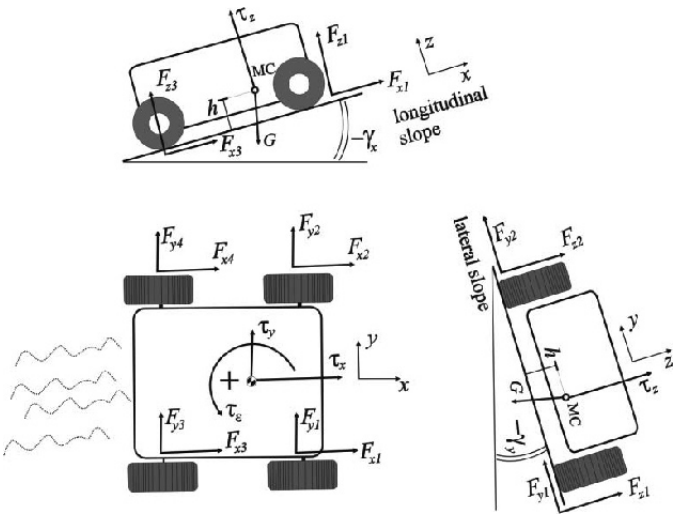

Figure 15.5. *4WD rover dynamic model – tire forces*

15.4.1. *Kinematical model*

Holonomic mechanisms are able to perform controlled movements through every available DoF within its particular task space. The non-holonomic mechanisms are capable of performing fewer controlled DoF than are actually available within its task space. A robot capable of differential (skid) steering, such as the rover presented in Figure 15.1, is able to move from one point to a different point and orientate within the same two-dimensional (2D) task space. However, it is only able to perform a single displacement (forward/backward) and a single rotation (turn, pivot or spin). Thus, it can execute only two controlled DoF, which is one less than the available (forward/backward, right/left and turn) in its task space. A kinematical model of the 4WD rover can be defined by the vector relation:

$$\begin{bmatrix} V \\ \dot{\varepsilon} \end{bmatrix} = \begin{bmatrix} r_t/2 & r_t/2 & r_t/2 & r_t/2 \\ \dfrac{r_t\cos(\zeta)}{d} & -\dfrac{r_t\cos(\zeta)}{d} & \dfrac{r_t\cos(\zeta)}{d} & -\dfrac{r_t\cos(\zeta)}{d} \end{bmatrix} \begin{bmatrix} \omega_1 \\ \omega_2 \\ \omega_3 \\ \omega_4 \end{bmatrix} \qquad [15.1]$$

where V and $\dot{\varepsilon}$ represents the forward (lump) speed and the robot yaw-rate, respectively; r_t is a tire radius, $\omega_i, i = 1,\ldots,4$ are particular tire angular

velocities; d is a geometry parameter, that is the corresponding planar distance of the robot tire centers from the robot geometry center *C*. The parameters used in the model presented in Figure 15.4 have the following meaning: t_r represents a track of the rover, l is the longitudinal distance between the front and rear wheel axes, l_x and l_y are corresponding distances of the body mass center (MC) from the rover geometry center C (point of crossing of the longitudinal and lateral axes) and h is the distance of the MC with respect to the ground surface (Figure 15.5).

Parameter d is calculated from the relation $d = 1/2 \cdot \sqrt{l^2 + t_r^2}$; angle ζ is the corresponding design-related parameter calculated from $tg(\zeta) = l / t_r$. The forward speed V has two components (Figure 15.4): the longitudinal $V_x \equiv \dot{x}$ and the lateral $V_y \equiv \dot{y}$. The speed is calculated from the equation:

$$V = \sqrt{\dot{x}^2 + \dot{y}^2} \qquad [15.2]$$

The tire kinematical model takes into account both – a tire rotation as well as a tire slipping on the ground surface. Consequently, the velocity vector of the *i*th tire v_i consists of two components: the slipping velocity $v_{s,i}$ and the speed $v_{r,i}$ due to a tire rotation (Figure 15.4). The slipping velocity $v_{s,i}$ depends not only on the tire revolution per minute (rpm) but also on the parameters of tire–ground interaction. The kinematical indices that represent a measure of tire slipping on the support surface in the longitudinal and lateral directions are known [ROD 02, PAC 93] as the tire slip ratio s_i and the tire slip angle α_i (Figure 15.4). The tire slip ratio and tire slip angle can be determined using the following kinematical relations [ROD 02, PAC 93]:

$$s_i = -\frac{v_{sx,i}}{v_{x,i}} = -\frac{v_{x,i} - v_{r,i}}{v_{x,i}} = -\frac{v_i \cos(\alpha_i) - r_i \omega_i}{v_i \cos(\alpha_i)}, \quad i = 1,\ldots,4 \qquad [15.3]$$

$$tg\,\alpha_i = -\frac{v_{sy,i}}{v_{x,i}}, \; i = 1,\ldots,4 \qquad [15.4]$$

The tire speed v_i (Figure 15.4) represents speed of motion of the *i*th tire MC. The tire slip angle α_i represents an angle defined with respect to the

longitudinal direction of motion (Figure 15.4). Only in an ideal case: the slipping velocity $v_{s,i}$ can be neglected and then it is assumed that the tires move by the speeds caused only by the rotation. The ideal case, for example, corresponds to the case of motion at low speed over a high frictional surface. The linear (translational) tire speeds $v_i, i = 1,\ldots,4$ are calculated from the following kinematical relations assuming the model presented in Figure 15.4:

$$\begin{aligned} v_1 &= \sqrt{(\dot{y} + l_f\dot{\varepsilon})^2 + (\dot{x} - t_r/2\ \ \dot{\varepsilon})^2} \\ v_2 &= \sqrt{(\dot{y} + l_f\dot{\varepsilon})^2 + (\dot{x} + t_r/2\ \ \dot{\varepsilon})^2} \\ v_3 &= \sqrt{(\dot{y} - l_r\dot{\varepsilon})^2 + (\dot{x} - t_r/2\ \ \dot{\varepsilon})^2} \\ v_4 &= \sqrt{(\dot{y} - l_r\dot{\varepsilon})^2 + (\dot{x} + t_r/2\ \ \dot{\varepsilon})^2} \end{aligned} \qquad [15.5]$$

where l_f and l_r represent corresponding geometry parameters shown in Figure 15.4. According to Figure 15.4, these lengths are $l_f = l_r = (1/2)\cdot l$. The directions of the particular tire speeds calculated in equation [15.6] are defined by the corresponding tire slip angles α_i calculated by use of the expressions:

$$\begin{aligned} tg(\alpha_1) &= \frac{\dot{y} + l_f\dot{\varepsilon}}{\dot{x} - t_r/2\,\dot{\varepsilon}}, \quad tg(\alpha_2) = \frac{\dot{y} + l_f\dot{\varepsilon}}{\dot{x} + t_r/2\,\dot{\varepsilon}} \\ tg(\alpha_3) &= \frac{\dot{y} - l_r\dot{\varepsilon}}{\dot{x} - t_r/2\,\dot{\varepsilon}}, \quad tg(\alpha_4) = \frac{\dot{y} - l_r\dot{\varepsilon}}{\dot{x} + t_r/2\,\dot{\varepsilon}} \end{aligned} \qquad [15.6]$$

15.4.2. *Model of robot dynamics*

The state vector of the considered robotic system (Figure 15.4) and its derivative are defined by the following relations:

$$\begin{aligned} q &= [x\ y\ z\ \varepsilon]^T \\ \dot{q} &= [\dot{x}\ \dot{y}\ \dot{z}\ \dot{\varepsilon}]^T \end{aligned} \qquad [15.7]$$

where x, y and z represent the coordinates of the robot MC defined with respect to the inertial coordinate system attached to the ground surface (see

Figure 15.4). Angle ε represents the corresponding yaw angle of the robot body about the z-axis. The robot dynamic model is defined in the state space in a way described in the following section.

15.4.2.1. *Robot rigid-body dynamics*

A 3D-model of the chosen robotic system (Figure 15.1) is presented in Figure 15.5. The model assumed describes robot dynamics with a satisfactory accuracy taking into account the most significant dynamic effects of the system. The model is presented in its general vector form:

$$T = H(q)\cdot\ddot{q} + h_{ccg}(q,\dot{q}) - F_w(\dot{q}) \qquad [15.8]$$

where $T \in \Re^{4\times 1}$ represents vector of the generalized forces and torques acting in the body MC. The generalized vector T has four components (Figure 15.5). T_x, T_y and T_z are generalized forces acting in the MC in longitudinal x, lateral y and z direction perpendicular to the ground support. The generalized torque T_ε produces spinning of the robot body about the z-axis; $H \in \Re^{4\times 4}$ is the inertia matrix; $h_{ccg} \in \Re^{4\times 1}$ is the vector of centrifugal, Coriolis and gravity forces and torque; $F_w \in \Re^{4\times 1}$ is the vector that includes the main external resistance forces (torque) such as: aerodynamic resistance, tire rolling resistances and Coulomb friction during a robotic motion. In order to achieve desired motion q and $\dot{q}$ defined in equation [15.7], the vector of the generalized forces and torque T, defined in [15.8], has to generate motion defined by the forward speed V and direction ε (robot cornering). In order to achieve desired forward speed and direction of motion, the robot has to produce corresponding tire forces and yaw torque τ in such a way to achieve that $T = \tau$. A vector that takes into account the tire forces (traction/braking and payload) and corresponding yaw moment that produces rover spinning about its z-axis is defined by:

$$\tau = \begin{bmatrix} \tau_x \\ \tau_y \\ \tau_z \\ \tau_\varepsilon \end{bmatrix} = \begin{bmatrix} \sum_{i=1}^{4} F_{xi} \\ \sum_{i=1}^{4} F_{yi} \\ \sum_{i=1}^{4} F_{zi} \\ M_z \end{bmatrix} \qquad [15.9]$$

$$M_z = \left(F_{x1} + F_{x3}\right)\cdot\left(\frac{t_r}{2} + l_y\right) - \left(F_{x2} + F_{x4}\right)\cdot\left(\frac{t_r}{2} - l_y\right) + \left(F_{y1} + F_{y2}\right)\cdot\left(l_f - l_x\right) - \left(F_{y3} + F_{y4}\right)\cdot\left(l_r + l_x\right), \quad [15.10]$$

where F_{x_i}, F_{y_i} $(i = 1,...,4)$ are corresponding longitudinal and lateral tire forces due to traction or braking (Figure 15.5). Tire load F_{zi} distribution depends on the distribution of robot masses as well as on the robot's position on a sloped surface (Figure 15.5).

The corresponding matrix and vectors of the model [15.8] are [ROD 02]:

$$H = \begin{bmatrix} m & 0 & 0 & 0 \\ 0 & m & 0 & 0 \\ 0 & 0 & m & 0 \\ 0 & 0 & 0 & I_z \end{bmatrix} \quad [15.11]$$

$$h_{ccg} = \begin{bmatrix} -m\ \dot{y}\ \dot{\varepsilon} + \dot{z}\ \dot{\gamma}_x + m\ g\ \sin(\gamma_x) \\ m\ \dot{x}\ \dot{\varepsilon} - \dot{z}\ \dot{\gamma}_y - m\ g\ \sin(\gamma_y)\ \cos(\gamma_x) \\ -\dot{x}\ \dot{\gamma}_x + \dot{y}\ \dot{\gamma}_y + m\ g\ \cos(\gamma_y)\ \cos(\gamma_x) \\ 0 \end{bmatrix} \quad [15.12]$$

where m is the lump mass of the robotic system, I_z is the robot's axial moment of inertia with respect to the z-axis and g is acceleration due to gravity. The total (resultant) resistance vector F_w including aerodynamic resistance, tire rolling resistance and Coulomb friction, is given below [ROD 02]:

$$F_w = \begin{bmatrix} -K_x\dot{x}^2 - \sum_{i=1}^{4} f_{r_i} F_{z_i} \cos\zeta_i \\ -K_y\dot{y}^2 - \sum_{i=1}^{4} f_{r_i} F_{z_i} \sin\zeta_i \\ 0 \\ \sum_{i=1}^{4} M_{\alpha i} \end{bmatrix}, \quad [15.13]$$

where K_x, K_y represents corresponding air resistance coefficients of the robot's body; $\sum_{i=1}^{4} M_{\alpha i}$ is sum of the tire self-aligning torques (tire resistance to

spinning about the *z*-axis) due to rover cornering; f_{r_i} is a rolling resistance coefficient of the particular *i*th tire and F_{z_i} represents corresponding tire payload depending on position of the MC (i.e. robot mass distribution) and the slope of a ground surface.

15.4.2.2. *Nonlinear tire model*

A considerable number of different models of tire force and moment-generating properties have been proposed in the available literature. The standard (proposed by the Society of Automotive Engineers (SAE)) in description of vehicle tire dynamics represents the so-called magic formula tire model originally introduced by Pacejka and Bakker [PAC 93]. The model provides a set of mathematical formulas from which the forces and moment acting from road to tire can be calculated at longitudinal and lateral slip conditions, which may occur simultaneously. The model aims at an accurate description of measured steady-state tire behavior. The coefficients of basic formula that are given in this section represent typifying quantities of the tire characteristic. By selecting proper values, the characteristics for either side force, aligning torque or fore and aft force can be obtained. The core of the nonlinear model is formed by the formula that has become known under the name "magic formula". This formula is capable of producing force and moment characteristics at pure slip conditions, that is either pure cornering or pure braking or driving. The formula (model) expresses the side force F_y, the aligning torque M_α and the longitudinal force F_x as a function of two arguments – the side slip angle defined by [15.4] and the longitudinal tire slip ratio determined by [15.3], respectively. The general form of the formula, which holds for a given value of vertical tire load, is:

$$f(u) = D \cdot \sin\left\{C \cdot arctg\left[B \cdot u - E \cdot \left(B \cdot u - arctg\left(B \cdot u\right)\right)\right]\right\} \qquad [15.14]$$

The empiric nonlinear Pacejka's tire model is shown in Figure 15.6. The magic formula $f(u)$ typically produces a curve that passes through the origin $u = f = 0,$ reaches a maximum and subsequently tends to a horizontal asymptote f_s (Figure 15.3). For constant coefficients B, C, D and E, the curve shows an antisymmetric shape with respect to the origin.

The formula is capable of producing characteristics that closely match measured curves for longitudinal F_x force, side (lateral) F_y force and self-aligning torque M_α as functions of their respective slip quantities: the slip

angle α [15.4] and longitudinal slip ratio s [15.3]. The output variable stands for either F_x, F_y or M_α and the input u may represent either s or α.

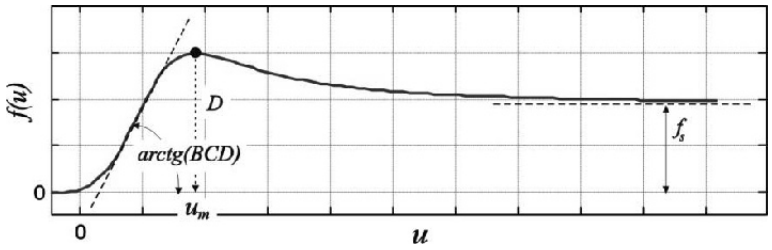

Figure 15.6. *General shape of the "magic formula" tire model to be used to describe tire nonlinear dynamics of the skid-steered 4WD rover (Figure 15.1)*

Figure 15.6 illustrates the meaning of some of the coefficients with the help of typical side force or longitudinal force characteristics [PAC 91, PAC 93, PAS 94]. Coefficient D (Figure 15.6) represents the peak value (with respect to the abscissa) and the product BCD corresponds to the slope at the origin $u = f = 0$. The factor C controls the limits of the range of the argument of the sine function. It thereby determines the shape of the resulting curve. Typical empirical values of the shape factor C are 1.30 for the side force F_y, 2.40 for the self-aligning torque M_α and 1.65 for the longitudinal (traction/brake) force F_x characteristic. The factor B is left to control the slope at the origin and is, therefore, called the stiffness factor. The remaining factor, *E*, appears to be necessary to influence the curvature near the peak of the curve. At the same time, E controls the slip u_m (Figure 15.6) at which the peak occurs (if present).

$$E = \frac{B \cdot u_m - tg\left(\frac{\pi}{2 \cdot C}\right)}{B \cdot u_m - arctg\left(B \cdot u_m\right)} \qquad [15.15]$$

The asymptotic value that $f(u)$ approaches at large slip values equals:

$$f_s = D \cdot \sin\left(\frac{\pi}{2} \cdot C\right) \qquad [15.16]$$

From these expressions, the initial values for C and E may be obtained for the least square regression procedure to acquire an optimal match to

measured data. More often, C is given a fixed value, typical for the kind of curve. A tire payload, that is tire torque that produces its rotation is calculated from:

$$\tau_t = F_x \cdot r_t \qquad [15.17]$$

where r_t is the tire radius. Tire payload τ_t as well as tire angular velocity (tire rpm) ω are used as feedback values for the servo-control of 4WD robot rover [SME 99, RAJ 78].

15.4.2.3. *Model of actuators*

DC motors are widely used as reliable actuators of mobile robots (Figure 15.1). According to [SME 99], the third-order mathematical model of a DC actuator can be written in the form:

$$\dot{x}_i = C_i \quad x_i + f_i \quad \hat{\tau}_i + d_i \quad N(u_i), \; i = 1,\ldots,4 \qquad [15.18]$$

where a 3D state vector for such system can be represented by:

$$x_i = \left[q_i \quad \dot{q}_i \quad i_{r_i} \right]^T, \quad i = 1,\ldots,4 \qquad [15.19]$$

The variables used in relations [15.18] and [15.19] have the following meaning: q_i and $\dot{q}_i$ are rotor position (angle) and angular velocity of the *i*th particular wheel actuator; i_{r_i} represents corresponding rotor current; $\hat{\tau}_i$ is the motor torque and $N(u_i)$ is the control voltage of a saturation type as defined in the following relation:

$$N(u_i) = \begin{cases} -u_{i,max} & \text{for} \quad u_i \le -u_{i,max} \\ u_i, & \text{for} \quad -u_{i,max} < u_i < u_{i,max} \\ u_{i,max} & \text{for} \quad u_i \ge u_{i,max} \end{cases} \qquad [15.20]$$

According to [SME 99], the system matrices are:

$$C_i = \begin{bmatrix} 0 & 1 & 0 \\ 0 & -B_C/J_r & C_M/J_r \\ 0 & -C_E/L_r & -R_r/L_r \end{bmatrix}; \; f_i = \begin{bmatrix} 0 \\ -1/J_r \\ 0 \end{bmatrix}; \; d_i = \begin{bmatrix} 0 \\ 0 \\ 1/L_r \end{bmatrix} \qquad [15.21]$$

Where C_M and C_E are the moment constant and the constant of electromotor force, L_r and R_r are the rotor inductivity and resistance, J_r is

the rotor moment of inertia, and B_C is the viscous friction coefficient reduced to the output shaft. Index "*i*" is omitted due to the simplification reasons.

15.5. Motion planning and control

The motion planning problem for non-holonomic systems, such as considered skid-steered 4WD rover (Figure 15.1), can be stated as follows: given a goal point in the environment with obstacles (mobile and immobile) in the workspace whose relative position (distance and azimuth angle) with respect to the robot is measurable, a robot subject to non-holonomic constraints, an initial configuration and a goal configuration and an admissible collision-free path between the initial and goal configurations are searched. Solving this problem requires us to take into account both the configuration space constraints due to obstacles and the non-holonomic constraints of the robotic system. The tools developed to address this issue thus combine motion planning and control theory techniques. In the following section, more details are given regarding the solution of these problems.

15.5.1. *Motion planning*

The objective of motion planning techniques is to compute a collision-free trajectory to the target configuration that complies with the vehicle constraints. This assumes a perfect model of the robot and scenario in advance. The advantage of these techniques is that they provide complete and global solutions of the problem. Nevertheless, when the surroundings are unknown and unpredictable, these techniques fail. One approach is to the map environment and to generate trajectories in real time [HAB 07], although these techniques are usually computationally expensive. A complementary way to address the motion problem in an unknown environment is obstacle avoidance. The objective is to move the vehicle toward a target location free of collisions with the obstacles detected by the sensors during motion execution. The advantage of reactive obstacle avoidance is to compute a motion by introducing the sensor information within the control loop, used to adapt the motion to any contingency incompatible with initial plans. The main cost of considering the reality of the world during operation is locality. In this instance, if global reasoning is required, a trap situation could occur. Despite this limitation, obstacle avoidance techniques are mandatory to deal with mobility problems in unknown and evolving surroundings.

The approach considered in this study assumes that the robot is equipped with corresponding proximity and range-finder sensors for detection of obstacles (as described in section 15.3.1) in surrounding, and that it operates in an informatically structured environment. This means that the robot is enabled to acquire satisfactory accurate information about its global position in the workspace and to determine a precise position of the robot target point in any time.

For accurate navigation and motion planning in the presence of obstacles, a robot needs to sense the following variables: (1) distance to surrounding obstacle(s), (2) its relative position with respect to obstacles (an angle calculated with respect to the robot longitudinal axis of symmetry), (3) relative position (azimuth angle) of the robot with respect to the target point and (4) in case of collision avoidance of mobile obstacle(s), a robot requires additional information regarding the obstacles speed of motion and direction in order to achieve a collision-free path. For motion planning with mobile robots, the fuzzy inference system (FIS) is an appropriate technique that enables accomplishing of such cognitive tasks. In this study, an FIS with two input and two output variables, similar to FIS in [MIT 10], is designed as the high-level motion planning module. The corresponding membership functions of the input variables are presented in Figure 15.7.

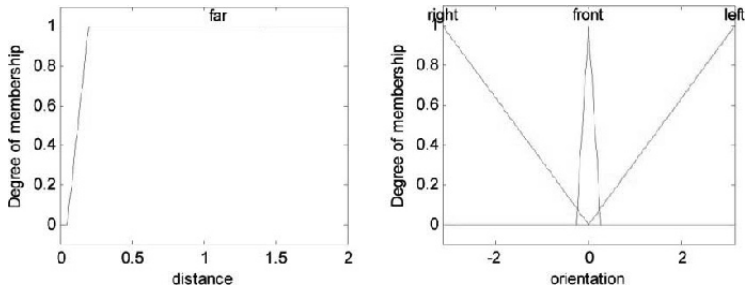

Figure 15.7. *Fuzzy membership functions of input variables "distance" and "orientation"*

The input variable "distance" possesses only one membership function "far", which is of a trapezoidal type with parameters $[0.05 \quad 0.1 \quad 2 \quad 2]$ (Figure 15.7). The input variable "orientation" is composed out of three membership functions: "right", "front" and "left" that are of a triangular type. Its parameters are $[-\pi \; -\pi \; 0]$, $[-\pi/10 \;\; 0 \;\; \pi/10]$ and $[0 \; \pi \; \pi]$, respectively (Figure 15.7).

The output membership functions of zero-order Sugeno-type fuzzy system are singletons (Table 15.1). For the output "velocity", fuzzy singletons (constants) are $V_{\max}$, V_{turn} and 0. For the output "angular velocity", constants are $-\omega$, 0 and ω.

	Velocity			Angular velocity		
	$V_{\max}$	V_{turn}	0	ω	0	$-\omega$
value	0.5 m/s	0.2 m/s	0 m/s	2 rad/s	0 rad/s	–2 rad/s

Table 15.1. *Fuzzy singleton values*

The assumed rules of the FIS base are as follows:

1) If "distance" is "far", and "orientation" is "right", then "velocity" is V_{turn} and "angular velocity" is ω.

2) If "distance" is "far", and "orientation" is "front", then "velocity" is $V_{\max}$ and "angular velocity" is 0.

3) If "distance" is "far", and "orientation" is "left", then "velocity" is V_{turn} and "angular velocity" is $-\omega$.

4) If "distance" is "not far", then "velocity" is 0 and "angular velocity" is 0.

The membership functions and the fuzzy rules are designed by using the Matlab®/Simulink Fuzzy Logic Toolbox [MAT 11].

Taking into account the generated output variables of the fuzzy path planner as well as bearing in mind the state variables of the system q and $\dot{q}$ defined by [15.7], a referent (desired) motion is possible to be defined. If the referent forward speed V_0 and the referent angular velocity (yaw rate) $\dot{\varepsilon}_0$ of the 4WD rover are assumed to be obtained from the fuzzy motion planning block, then the referent state variables q_0, $\dot{q}_0$ and $\ddot{q}_0$ of the system can be established in the following way [ROD 10b]:

$$\begin{aligned} \dot{x}_0 &= V_0 \ \cos(\varepsilon_0) \\ \dot{y}_0 &= V_0 \ \sin(\varepsilon_0) \\ \dot{\varepsilon}_0 &= \dot{\varepsilon}_0 \end{aligned} \qquad [15.22]$$

where ε_0 is the referent, that is nominal yaw angle determined previously from the expression:

$$\varepsilon_0 = \int \dot{\varepsilon}_0 \cdot dt, \quad t \in (0, \mathrm{T}] \qquad [15.23]$$

The vector of nominal speed values $\dot{q}_0$ of the robotic system has the form:

$$\dot{q}_0 = \begin{bmatrix} \dot{x}_0 & \dot{y}_0 & 0 & \dot{\varepsilon}_0 \end{bmatrix}^T \qquad [15.24]$$

and the corresponding vector of the nominal accelerations is obtained by derivation of [15.24]:

$$\ddot{q}_0 = \frac{d\,\dot{q}_0}{dt} \qquad [15.25]$$

The main task of a robot controller is to ensure that the actual robot motion $q(t), t \in (0, T]$ converges to the nominal motion $q_0(t), t \in (0, T]$ as well as to enable satisfactory dynamic behavior of the robotic system even in the presence of system uncertainties and perturbations of different types.

15.5.2. *Motion control*

The control architecture of the 4WD robot rover (Figure 15.1) represents a modular hierarchy distributed structure (Figures 15.2 and 15.3). The proposed control architecture has two hierarchy levels – high level and low level [ROD 10b]. The high control level consists of a cognitive block (the fuzzy motion planning module, described in section 15.5.1) coupled with the complementary model-based dynamic controller. The controller takes into account dynamics of the entire system including robot rigid-body dynamics, tire nonlinear dynamics and dynamics of rover actuators described in equations [15.7–15.21]. The high control level block is charged with sensor-data acquisition and sensor-data fusion, signal processing, navigation and motion planning, control of robot dynamic behavior as well as distribution of control commands per particular robot wheels. A rover servo-control (low-level control) ensures appropriate power-driving according to the high-level control commands and driving conditions. The control system considered in

this study has a "distributed" character due to the reasons explained earlier. The low control variables represent corresponding tire torques and tire rpm (angular velocities) determined according to the actual tire–ground conditions as well as according to the referent robot motion. In such a way, the control system designed "takes care" about robot dynamics under real (variable) driving conditions.

The controller was designed under the following assumptions:

1) The model presented in this chapter by equations [15.1–15.21] describes the system's physical behavior, with satisfactory accuracy being the main physical effects taken into account.

2) Parameters of the model can be determined in a precise way. The parameters are acquired from the CAD model or directly from the system by measurement (mass, moments of inertia, geometry parameters, etc.) or by estimation using corresponding sensorial information, a model of the system and a Kalman filter.

3) Corresponding tire–ground interaction parameters (slipping and rolling resistance coefficients) can be identified with satisfactory precision by using the tire nonlinear empirical model [15.14–15.17] and corresponding measurement data regarding the tire torques and a tire rpm.

Taking into account the previous consideration, the high-level control algorithm has to ensure accurate path tracking of the reference trajectory (obtained from the fuzzy motion planning module) and fine dynamic performances of the system. The control algorithm capable of achieving these requirements is derived in the following form using the robot model [15.8]:

$$\begin{aligned}
T_x &= H^{(1)}(q)\cdot\left[\ddot{x}_0 - k_d^{(1)}\ \left(\dot{x}-\dot{x}_0\right) - k_p^{(1)}\left(x-x_0\right)\right] + h_{ccg}^{(1)}(q,\dot{q}) - F_w^{(1)}(q)\\
T_y &= H^{(2)}(q)\cdot\ddot{y} + h_{ccg}^{(2)}(q,\dot{q}) - F_w^{(2)}(q)\\
T_z &= H^{(3)}(q)\cdot\ddot{z} + h_{ccg}^{(3)}(q,\dot{q}) - F_w^{(3)}(q)\\
T_\varepsilon &= H^{(4)}(q)\cdot\left[\ddot{\varepsilon}_0 - k_d^{(4)}\ \left(\dot{\varepsilon}-\dot{\varepsilon}_0\right) - k_p^{(4)}\left(\varepsilon-\varepsilon_0\right)\right] + h_{ccg}^{(4)}(q,\dot{q}) - F_w^{(4)}(q)
\end{aligned} \qquad [15.26]$$

where $k_p^{(i)}$ and $k_d^{(i)}, i=1,\ldots,4$ are corresponding proportional and differential control gains in the particular directions (longitudinal and yaw) of motion. $H^{(i)}$, $h_{ccg}^{(i)}$ and $F_w^{(i)}, i=1,\ldots,4$ are corresponding *i*th row, that is *i*th elements of H, h_{ccg} and F_w from model [15.8]. As has been explained in

section 15.3.1, the 4WD robot (Figure 15.1), as a non-holonomic system, is only able to perform a single displacement (forward or backward) and a single yaw rotation (turn). Thus, it can accomplish only two controlled DoF. Bearing this fact in mind, the robot (Figure 15.1) is controlled in an explicit way in the longitudinal (x) and yaw (ε) directions while in the other two coordinate directions (y and z) the rover is controlled implicitly [15.26]). The corresponding driving forces τ_x and torques τ_ε in the particular longitudinal and yaw directions are determined from:

$$\tau_x = T_x, \quad \tau_\varepsilon = T_\varepsilon \qquad [15.27]$$

The driving forces τ_x and torques τ_ε, calculated in [15.27], are generated by the corresponding tire forces F_{xi} and $F_{yi}, i = 1,\ldots,4$ (Figure 15.5). In that sense, 4WD rover represents an "over controlled" system since there are four controlled tire forces $F_{xi}, i = 1,\ldots,4$ (lateral tire forces are not controlled in an explicit way) that should produce robotic motion in two controlled directions: longitudinal and yaw. The unknown tire forces F_{xi} can be determined from the system of equations [15.9] and [15.10] by imposing certain additional simplifications. Aiming at this, it is assumed that the right-side tires and the left-side tires (front and rear) rotate at the same speed (rpm). Through this assumption, the number of unknown variables $F_{xi}, i = 1,\ldots,4$ can be reduced twice. Assuming the previous assumption as well as the fact that the longitudinal forces $F_{xi}, i = 1,\ldots,4$ and the tire loads $F_{zi}, i = 1,\ldots,4$ correlate, the following auxiliary relations can be set as:

$$F_{x3} = \frac{F_{z1}}{F_{z3}} F_{x1}, \quad F_{x4} = \frac{F_{z2}}{F_{z4}} F_{x2} \qquad [15.28]$$

The payload forces $F_{zi}, i = 1,\ldots,4$ are determined either directly by measurement at the robots tires (advance designs) or by calculation, taking into account a relative position of the robot body MC with respect to the geometry center C (Figure 15.4), and implementing a matrix of transformation regarding the case when the robot moves on the sloped surface. From relations [15.9] and [15.10], taking into account simplification [15.28] as the auxiliary relation, the system of two linear equations is derived. It enables determining the unknown tire forces $F_{xi}, i = 1,\ldots,4$. The mentioned system of linear equations has the form:

$$\tau_x = F_{x1}\left(1+\frac{F_{z1}}{F_{z3}}\right)+F_{x2}\left(1+\frac{F_{z2}}{F_{z4}}\right)$$
$$\tau_\varepsilon = F_{x1}\left(1+\frac{F_{z1}}{F_{z3}}\right)\left(\frac{t_r}{2}+l_y\right)-F_{x2}\left(1+\frac{F_{z2}}{F_{z4}}\right)\left(\frac{t_r}{2}-l_y\right)+A_\varepsilon \qquad [15.29]$$
$$A_\varepsilon = \left(F_{y1}+F_{y2}\right)\cdot\left(l_f-l_x\right)-\left(F_{y3}+F_{y4}\right)\cdot\left(l_r+l_x\right)$$

where A_ε is a residual term that includes actual values of the lateral tire forces $F_{yi}, i=1,\ldots,4$. The searched variables ($F_{xi}, i=1,\ldots,4$) are used afterward for calculation of the particular tire speeds (rpm) $\omega_i, i=1,\ldots,4.$ For this purpose, the empirical tire model defined by relations [15.14–15.16] is utilized. Prior to determination of the tire rpm, the corresponding tire slip ratios s_i [15.3] and tire slip angles α_i [15.4] have to be identified that enable the final estimation of the controlled values of the tire speeds $\omega_i, i=1,\ldots,4.$

Following the unique procedure of control variables calculation, tire torques τ_t (torques at the gear box shaft) are calculated by using [15.17]. Then, the reference values of the servo-controller are defined, using actuator model equations [15.18–15.21] and including the variables (tire torque τ_t and tire angular speed ω) calculated earlier. The procedure of control variables calculation results in controlled voltage of the DC motors at the end. Navigation, motion planning and control algorithms proposed in this study, considered in section 15.5, are verified by utilization of the appropriate software simulator as well as experimentally using the open-structure wheel-based robotic platform presented in Figure 15.1.

15.6. Simulation and experimental testing

The open-structure mobile robotic platform considered in this chapter is experimentally tested within the context of a networked system. Wireless robot-sensor networked (WRSN) systems refer to multiple robots operating together in coordination or cooperatively with sensors, embedded computers and human operators [MOR 08]. Cooperation entails more than one entity working toward a common goal while coordination implies a relationship between entities that ensures efficiency or harmony. Wireless communication between entities and advanced sensing are fundamental to both cooperation and coordination and hence the central role of the networked system. Networked robots allow multiple robots and auxiliary entities to perform

tasks that are well beyond the abilities of a single robot. Tasks such as searching or mapping, in principle, are performed faster with an increase in the number of robots. Perhaps the biggest advantage of using the network to connect robots is the ability to connect and harness physically removed assets. Mobile robots can react to information sensed by other mobile robots in the next room.

Bearing in mind the enormous importance of building and use of such WRSN systems, the necessities of accurate modeling, appropriate experimental testing and verification are unavoidable steps in design and development of such kinds of complex systems and their robot entities. One such system, developed in laboratory conditions [ROD 11], is used for experimental testing of navigation, motion planning and control algorithms considered in this chapter. A panoramic view to the experimental WRSN system developed is presented in Figure 15.8. Prior to the experimental validation of the algorithms designed and considered in this chapter, corresponding simulation experiments are needed in order to enable initial tuning of the system, testing of dynamic characteristics and analysis of system performances assuming the checking of the system robustness to different parametric and system uncertainties. In that sense, a model of an arbitrary, realistic multi-robot scenario, suitable for extensive simulation testing of different case studies regarding autonomous navigation, motion planning and control in the presence of obstacles (mobile and immobile), is used [ROD 10a]. The main screen presenting the graphical interface of modeling multi-robots scenario is shown in Figure 15.9.

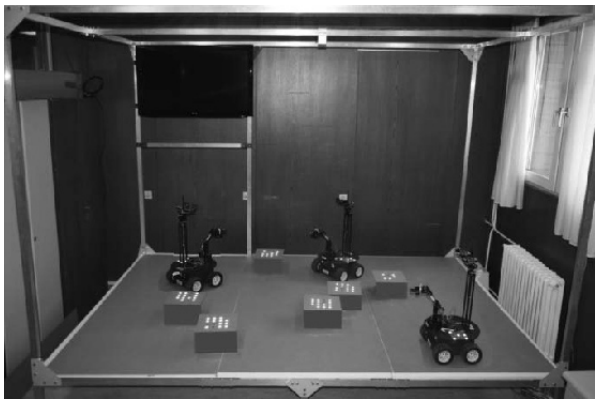

Figure 15.8. *Experimental test-bed station for research, development and benchmarking of motion planning and control algorithms designed for networked robotic systems*

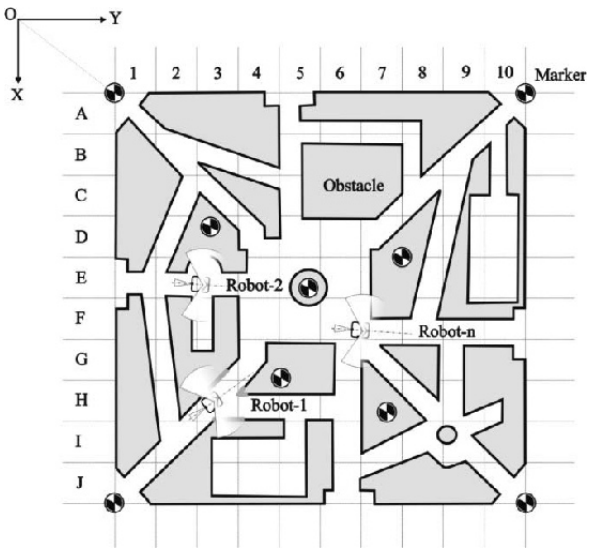

Figure 15.9. *Virtual WRSN – software simulator [ROD 10a], user-friendly graphical interface that enables imposing and simulation of multi-robot dynamic scenarios*

15.6.1. *Case studies*

In order to illustrate the proposed methodology of motion planning and control with a 4WD mobile robot (Figure 15.1), two typical case studies are analyzed: (1) motion of a single robot in the presence of stationary (immobile) obstacles, and (2) collision avoidance with mobile obstacles. Both scenarios are tested by using the simulator (Figure 15.9) as well as experimentally in a manner presented in Figure 15.8. In the considered cases, trajectory tracking accuracy as well as robot dynamic performances are evaluated.

The indoor mobile robot (Figure 15.1) is simulated. The parameters of the robot and tires were identified directly on the system by appropriate measurement or by estimation using the model defined in section 15.3. The parameters used in simulation are given in the Appendix. The robot is simulated moving in an unknown and unstructured environment (a labyrinth scenario, Figure 15.9) with uncertainty of tire–ground interaction (slippery surface). The imposed range of motion is assumed to be a square area of 15 m × 15 m with the radial and transversal narrow corridors whose width is less than 1 m. The robot is required to move with a safe speed avoiding the stationary obstacles as shown in

Figure 15.9. The "Virtual WRSN", a specialized Matlab®/Simulink toolbox, is used for simulation testing [ROD 10a].

The motion planning module (fuzzy block) and the corresponding dynamic controller are required to "find the shortest collision-free path" and to achieve desired motion in a way that ensures satisfactory dynamic behavior of the system. Characteristic simulation results, which contribute to the case-based analysis, are presented in Figures 15.10–15.13. The proposed algorithms of navigation and control ensure obstacle avoidance with a satisfactory precision even in an unknown and unstructured environment (Figure 15.10). The skid steering effects are shown in Figures 15.11 and 15.12. The longitudinal (traction/braking) tire forces are generated and changed independently on the robot wheels based on estimation of tire–ground adhesion parameters (using tire model and corresponding measurements of tire load). In such a way, lateral slipping and angular driftage of the robot are suspended (reduced to minimum) and this caused a smooth motion (no jerks). The smooth forward velocity profile and tire angular speeds (Figure 15.12) prove that the applied controller ensures reliable motion and fine dynamic behavior of the system. The control voltages of the DC motors are presented in Figure 15.13. The obtained voltages do not overcome the maximal range of 12 V. It proves that the control algorithm synthesized in this case fits well, both – the robot dynamics and also the tire–ground dynamics.

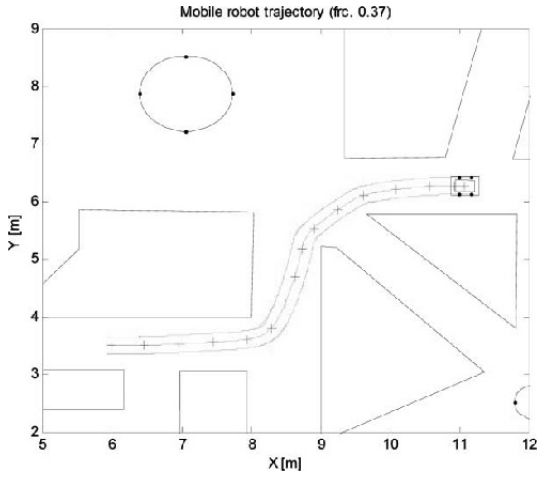

Figure 15.10. *Example of the test scenario of obstacle avoidance in an unknown and unstructured environment using "Virtual WRSN" software simulator [ROD 10a]*

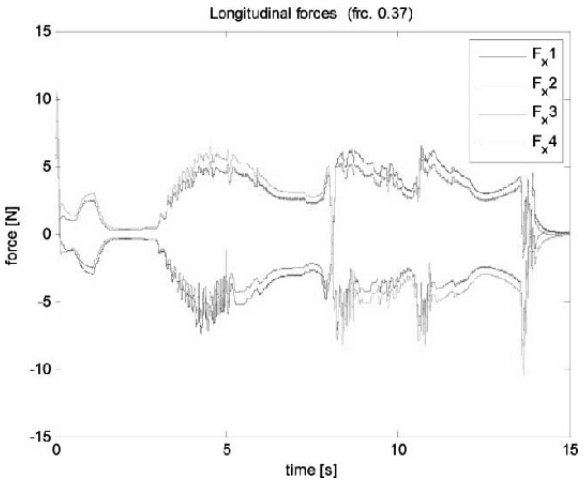

Figure 15.11. *Longitudinal tire forces achieved during the avoiding scenario (Figure 15.10)*

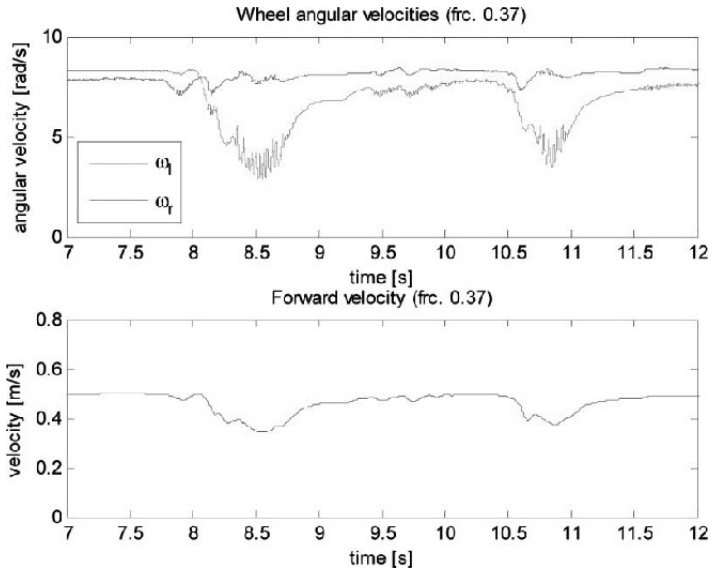

Figure 15.12. *Actual forward speed and corresponding tire angular velocities (right and left side) achieved in the interval 7–12 s of a robot changing direction ("S" maneuver). For a color version of this figure please see www.iste.co.uk/mechatroneng.zip*

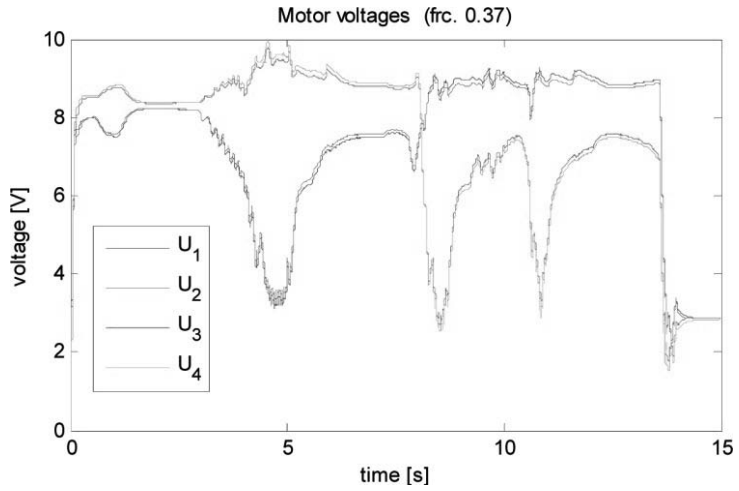

Figure 15.13. *Control voltages of robot actuators (DC motors) generated to enable desired motion presented in Figure 15.10.*

In the second case study, a dynamic multi-robot scenario of collision avoidance is simulated under the same conditions as in the previous case. Four robots with the same characteristics (kinematical and dynamic parameters) are used in the test. The robots are required to move independently in the small area intersecting their expected trajectories (Figure 15.14). The Coulomb friction coefficient of the ground surface is set to $\mu = 0.37$ as in the previous case study. The fuzzy motion planning modules of the particular robots have the tasks to identify the fastest collision-free trajectories and to enable reaching the target points with satisfactory precision. The concurrent robots are neither communicated between themselves nor in an indirect way by the basis station. The robots are restricted to use only their proximity and range sensors to detect mobile and immobile obstacles in their surroundings. The obtained simulation results are shown in Figures 15.14 and 15.15. The snapshots of the mobile robots in the particular characteristic sequences of motion are presented per second. From the plots shown in Figure 15.14, the way of obstacle avoidance among the moving robots can be observed by analyzing few characteristic time sequences. Particular robots, shown in the plots, stop and wait (Figure 15.15) for another robot(s) to pass away or they change the paths on-line to avoid collisions.

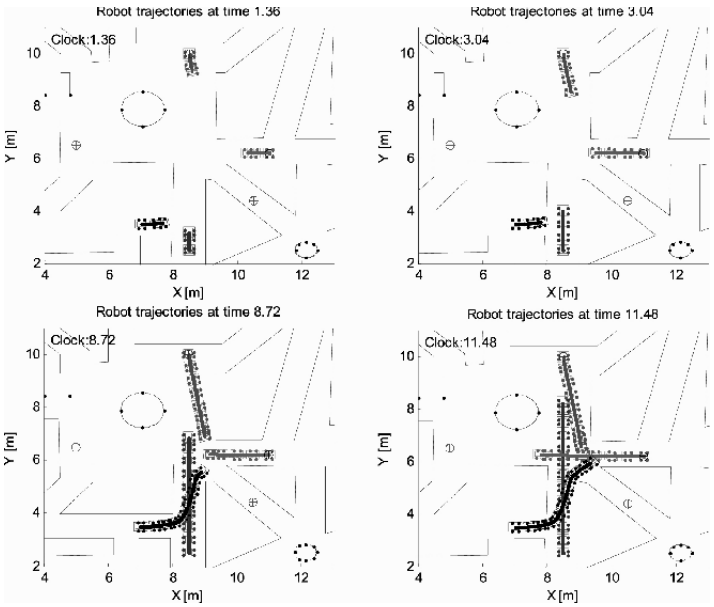

Figure 15.14. *The snapshots of robots in a collision avoidance scenario captured at 1.38, 3.04, 8.72 and 11.48 s from the start of motion*

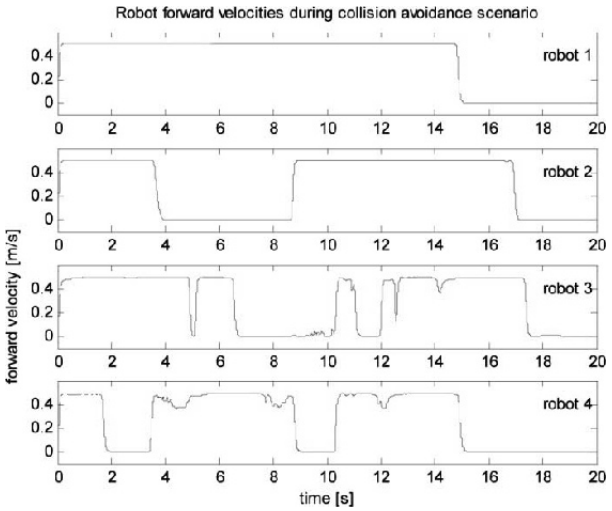

Figure 15.15. *Time history plots of the forward speeds of the participating robots in the considered collision avoidance scenario presented in Figure 15.14.*

15.7. Concluding remarks

The main contribution of this chapter is the development of an open-structure wheel-based mobile robotic platform and a complementary software simulator aimed at research, the development and education, as well as the objective benchmarking of this kind of advanced mechatronics system. The main objectives of the work are concerned with solving the problems of development of an autonomous navigation system, motion planning and control of mobile robots in unstructured environments in the presence of mobile and immobile obstacles and system uncertainties such as variation of tire–ground interaction performances. The described 4WD robotic system of an open structure as well as its extension to the wireless robot and sensor networked system (the unique test-bed station, Figure 15.8) offer great opportunities for research, analysis and objective benchmarking of such kinds robotic systems. Navigation, motion planning and control algorithms (including wireless communication) are of special interest for reliable and safe operation of the considered mechatronic system in the scope of an informatically structured environment. The complementary software simulator "Virtual WRSN" was also developed in order to support research and development and to speed up improvements of system performances. Both, the software simulator as well as the experimental test-bed station with the open-structure mobile robotic platform included represent useful research and engineering tools that can significantly simplify and speed up the designing process. Also, the system developed represents a scalable and a cost-effective mechatronic system whose architecture can be utilized for building advance industrial mobile wheel-based robotic platforms. Bearing in mind the aforementioned facts, advanced mechatronic systems of open structures, such as the system presented in this chapter, play a significant role in objective benchmarking and performance evaluation of various types of navigation and control algorithms designed for such robotic devices. Appropriate objective benchmarking and experimental system evaluation, under different unpredictable conditions of system operation, represent, today, the ultimate requirement for system performance optimization. This chapter represents a contribution in that sense.

The chosen case studies considered in this chapter have been used to illustrate the proposed methodology of motion planning and control of wheel-based robot dynamics in unknown environment with the disturbance of tire–ground parameters' uncertainty type. The same robot (model and experimental system) was used for evaluation of different control algorithms aiming to achieve the best dynamic performances of the system in the

presence of mobile and immobile obstacles as well as in the case of the slippery surface. A corresponding performance analysis was done and the dynamic control (skid steering) is favored with respect to the kinematical control based on simplified differential steering approach. The drawbacks of the kinematical approach are the missing information about the robot dynamics and tire–ground interactions.

15.8. Acknowledgments

The study presented in this chapter represents results of the national research project "Ambientally intelligent service robots of anthropomorphic characteristics" TR-35003 supported by the Serbian Ministry of Education and Science and partially supported by the SNSF-SCOPES "CARE-robotics" project no. IZ74Z0_137361/1.

15.9. Bibliography

[ADL 11] ADLS15PC – PC104-Plus Embedded single board computer, Advanced digital logic, 2011. Available at http://www.adl-usa.com.

[AZA 94] AZARM K., SCHMIDT G., "Integrated mobile robot motion planning and execution in changing indoor environments", *Proceedings of the IEEE/RSJ International Conference on Intelligent Robots and Systems IROS'94*, Munich, Germany, pp. 298–305, 12–16 September 1994.

[BOR 89] BORENSTEIN J., KOREN Y., "Real-time obstacle avoidance for fast mobile robots", *IEEE Transaction on System Man and Cybernetics*, vol. 19, no. 5, pp. 1179–1187, 1989.

[BOR 91] BORENSTEIN J., KOREN Y., "The vector field histogram – fast obstacle avoidance for mobile robots", *IEEE Transaction on Robotics and Automation*, vol. 7, no. 3, pp. 278–288, 1991.

[CAR 99] CARACCIOLO L., LUCA A.D., IANNITTI S., "Trajectory tracking control of a four-wheel differentially driven mobile robot", *Proceedings of the IEEE International Conference on Robotics and Automation ICRA'99*, Detroit, Michigan, pp. 2632–2638, 10–15 May 1999.

[CHA 82] CHATILA R., "Path planning and environmental learning in a mobile robot system", *Proceedings of the European Conference on Artificial Intelligence ECAI'82*, Orsay, France, pp. 112–118, 12–14 July 1982.

[CHA 85] CHATTERGY R., "Some heuristics for the navigation of a robot", *International Journal of Robotic Research*, vol. 4, no. 1, pp. 59–66, 1985.

[DEV 11] DEVENTECH, ultrasonic range finder, 2011. Available at http://www.robotshop.com.

[DFR 11] DFROBOT, 4WD outdoor mobile platform, 2011. Available at http://www.robotshop.com.

[FEI 94] FEITEN W., BAUER R., LAWITZKY G., "Robust obstacle avoidance in unknown and cramped environments", *Proceedings of the IEEE International Conference on Robotics and Automation ICRA'94*, San Diego, CA, pp. 2412–2417, 8–13 May 1994.

[FIO 98] FIORINI P., SHILLER Z., "Motion planning in dynamic environments using velocity obstacles", *International Journal of Robotic Research*, vol. 17, no. 7, pp. 760–772, 1998.

[FOX 97] FOX D., BURGARD W., THRUN S., "The dynamic window approach to collision avoidance", *IEEE Robotics and Automation Magazine*, vol. 4, no. 1, pp. 23–33, 1997.

[HAB 06] HABIB M.K., "Mechatronics engineering the evolution, the needs and the challenges", *Proceedings of the 32nd Annual Conference on IEEE Industrial Electronics Society IECON 2006*, Paris, France, pp. 4510–4515, 6–10 November 2006.

[HAB 07] HABIB M.K., "Real time mapping and dynamic navigation for mobile robots", *International Journal of Advanced Robotic Systems*, vol. 4, no. 3, pp. 323–338, 2007.

[KHA 86] KHATIB O., "Real-time obstacle avoidance for manipulators and mobile robots", *International Journal of Robotic Research*, vol. 5, no. 1, pp. 90–98, 1986.

[KOZ 04] KOZLOWSKI K., PAZDERSKI D., "Modeling and control of a 4-wheel skid-steering mobile robot", *International Journal of Applied Mathematics and Computer Science*, vol. 14, no. 4, pp. 477–496, 2004.

[KRO 86] KROGH B.H., THORPE C.E., "Integrated path planning and dynamic steering control for autonomous mobile robots", *Proceedings of the IEEE International Conference on Robotics and Automation ICRA'86*, San Francisco, CA, pp. 1664–1669, 7–10 April 1986.

[LUM 87] LUMELSKY V., STEPANOV A., "Path planning strategies for a point mobile automation moving amidst unknown obstacles of arbitrary shape", *Algorithmica*, vol. 2, no. 4, pp. 403–430, 1987.

[LYN 11] LYNXMOTION, AL5A 4 Degrees of freedom robotic arm Combo kit, 2011. Available at http://www.lynxmotion.com.

[MAS 94] MASOUD A., MASOUD S., BAYOUMI M., "Robot navigation using a pressure generated mechanical stress field – the biharmonical potential approach", *Proceedings of the IEEE International Conference on Robotics and Automation ICRA'94*, San Diego, CA, pp. 124–129, 8–13 May 1994.

[MAT 11] MATHWORKS, Matlab/Simulink, Fuzzy toolbox – user manual, 2011. Available at http://www.mathworks.com/products/fuzzylogic.

[MIN 00] MINGUEZ J., MONTANO L., "Nearness diagram (ND) navigation: collision avoidance in troublesome scenarios", *IEEE Transactions on Robotics and Automation*, vol. 20, no. 1, pp. 45–59, 2000.

[MIN 04] MINGUEZ J., OSUNA J., MONTANO L., "A divide and conquer strategy to achieve reactive collision navigation systems", *Proceedings of the IEEE International Conference on Robotics and Automation ICRA 2004*, New Orleans, LA, 26 pp. 412–418, April–May 2004.

[MIN 05] MINGUEZ J., "The obstacle-restriction method for robot obstacle avoidance in difficult environments", *Proceedings of the IEEE International Conference on Intelligent Robots and Systems IROS 2005*, Alberta, Canada, pp. 2284–2290, 2–6 August 2005.

[MIN 08] MINGUEZ J., LAMIRAUX F., LAUMOND J.-P., "Motion planning and obstacle avoidance", *Handbook of Robotics*, Springer, Berlin, pp. 826–850, 2008.

[MIN 11] MINDSENSORS, infrared and light sensors, 2011. Available at http://www.robotshop.com.

[MIT 10] MITROVIĆ S., ĐUROVIĆ Ž., "Fuzzy logic controller for bidirectional garaging of a differential drive mobile robot", *Advanced Robotics*, vol. 24, nos. 8–9, pp. 1291–1311, 2010.

[MOR 08] MORIN P., SAMSON C., "Motion control of wheeled mobile robots", *Handbook of Robotics*, Springer, Berlin, pp. 729–825, 2008.

[PAC 91] PACEJKA H.B., SHARP R.S., "Shear force development by pneumatic tires in steady state conditions: a review of modeling aspects", *Vehicle System Dynamics: International Journal of Vehicle Mechanics and Mobility*, vol. 20, nos. 3–4, pp. 121–175, 1991.

[PAC 93] PACEJKA H., BAKKER B., "The magic formula tire model", *Vehicle System Dynamics: International Journal of Vehicle Mechanics and Mobility*, vol. 21, suppl. 001, pp. 1–18, 1993.

[PAS 94] PASTERKAMP W.R., PACEJKA H.B., "On line estimation of tire characteristics for vehicle control", *Proceedings of the International Symposium on Advanced Vehicle Control AVEC'94*, Tsukuba, Japan, pp. 521–526, 24–28 October 1994.

[RAJ 78] RAJARAM S., MURUGESAN S., "A new method for speed measurement/control of DC motors", *IEEE Transactions on Instrumentation and Measurement*, vol. 27, no. 1, pp. 99–102, 1978.

[ROD 02] RODIĆ A., VUKOBRATOVIĆ M., *Dynamics, Integrated Control and Stability of Automated Road Vehicles*, Ibidem Verlag, Stuttgart, 2002.

[ROD 10a] RODIĆ A., MESTER G., "Virtual WRSN – modeling and simulation of wireless robot-Sensor networked systems", *Proceedings of the 8th International Symposium on Intelligent Systems and Informatics SISY 2010*, Subotica, Serbia, pp. 115–120, 10–11 September 2010.

[ROD 10b] RODIĆ A., ADDI K., JEZDIMIROVIĆ M., "Sensor-based intelligent navigation and control of autonomous mobile robots in advanced terrain missions", *Scientific Technical Review*, vol. 60, no. 2, pp. 7–15, 2010.

[ROD 11] RODIĆ A., JOVANOVIĆ M., POPIĆ S., *et al*., "Scalable experimental platform for research, development and testing of networked robotic systems in informationally structured environments", *IEEE Symposium Series on Computational Intelligence SSCI 2011*, Paris, France, pp. 136–143, 11–15 April 2011.

[RYU 11] RYU J.C., AGRAWAL S.K., "Differential flatness-based robust control of mobile robots in the presence of slip", *The International Journal of Robotics Research*, vol. 30, no. 4, pp. 463–475, 2011.

[SIM 96] SIMMONS R., "The curvature-velocity method for local obstacle avoidance", *Proceedings of the IEEE International Conference on Robotics and Automation ICRA'96*, Minneapolis, MN, pp. 3375–3382, 22–28 April 1996.

[SIN 96] SINGH L., STEPHANOU H., WEN J., "Real-time robot motion control with circulatory fields", *Proceedings of the IEEE International Conference on Robotics and Automation ICRA'96*, Minneapolis, MN, pp. 2737–2742, 22–28 April 1996.

[SME 99] SMEATON R.W., *Switchgear and Control Handbook*, 3rd ed., McGraw Hill, New York, 1999.

[STA 11] HAGISONIC, StarGazer – infrared localization system, 2011. Available at http://www.hagisonic.com/.

[STR 84] STRATEGIESL L., "Strategies for solving collision-free trajectories problems for mobile robots and manipulator robots", *International Journal of Robotic Research*, vol. 3, no. 4, pp. 51–65, 1984.

[SUR 11] Surveyor Stereo Vision System, Surveyor Corporation, 2011. Available at http://www.surveyor.com.

[WAR 08] WARD C.C., IAGNEMMA K., "A dynamic-model-based wheel slip detector for mobile robots on outdoor terrain", *IEEE Transactions on Robotics*, vol. 24, no. 4, pp. 821–831, 2008.

[WIK] WIKIPEDIA, Ackermann steering geometry, http://en.wikipedia.org/wiki/Ackermann_steering_geometry

[YI 07] YI J., SONG D., ZHANG J., *et al*., "Adaptive trajectory tracking control of skid-steered mobile robots", *Proceedings of the IEEE International Conference on Robotics and Automation ICRA 2007*, Rome, Italy, pp. 2605–2610, 10–14 April 2007.

15.10. Appendix

In addition to the study presented in the chapter, parameters used in simulation of case studies are presented in Table A1.1. Values of parameters are taken from the product sheet, or estimated by use of the model.

Parameter	Symbol	Value	Unit
Wheel radius	r_t	0.06	m
Front wheel distance	l_f	0.082	m
Vehicle track	t_r	0.29	m
Rear wheel distance	l_r	0.1	m
MC displacement in x	l_x	0.018	m
MC displacement in y	l_y	0	m
Mass	m	6.8	kg
Moment of inertia	I_z	0.0921	kgm^2
Gravity	g	9.81	m/s^2
Air resistance in x	K_x	1.36	Ns^2/m^2
Air resistance in y	K_y	1.50	Ns^2/m^2
Rolling friction	f_{ri}	0.02	–
Tire model coefficient	B	0.1884	–
Tire model coefficient	C	1.30	–
Tire model coefficient	D	38.84	N
Tire model coefficient	E	-2.8556×10^5	–
Rotor inductance	L_r	94×10^{-6}	H
Rotor resistance	R_r	2.35	Ω
Rotor inertia	J_r	50×10^{-9}	kgm^2
Viscous friction	B_C	1.1×10^{-6}	Ns/m
Reduction gear	N	67	–
Voltage constant	C_M	15×10^{-3}	Vs/rad
Torque constant	C_E	15×10^{-3}	Nm/A

Table A1.1. *Parameters of 4WD rover, and their values used in simulation of case studies*